Copyright Notice

Institute of Communication Networks and Computer Engineering
University of Stuttgart
Pfaffenwaldring 47, D-70569 Stuttgart, Germany
Phone: ++49-711-685-68026, Fax: ++49-711-685-67983
Email: mail@ikr.uni-stuttgart.de, http://www.ikr.uni-stuttgart.de

Performance Analysis of Adaptive Hybrid ARQ for Inter-HAP Free-Space Optical Fading Channel with Delayed Channel State Information

Swaminathan Parthasarathy[a] (swaminathan.parthasarathy@dlr.de), Andreas Kirstädter[b] (andreas.kirstaedter@ikr.uni-stuttgart.de), Dirk Giggenbach[a] (dirk.giggenbach@dlr.de)
[a]Institute of Communications and Navigation, German Aerospace Centre (DLR), D-82234 Wessling;
[b]Institute of Communication Networks and Computer Engineering, University of Stuttgart, D-70569 Stuttgart

Abstract

In this paper, we present simulative performance analysis of Hybrid Automatic Repeat reQuest (ARQ) with adaptive rate Reed-Solomon (RS) code under delayed Channel State Information (CSI) at the transmitter over inter-HAP (High Altitude Platform) FSO fading channel. The combined effect of atmospheric turbulence and temporal behaviour of the channel were investigated. The performance analysis is determined in terms of Transmission Efficiency (TE) via event based simulations. The results enable us to analyse the benefit of adaptive rate HARQ in presence of delayed CSI so as to maximize the transmission efficiency.

1 Introduction

Free Space Optical (FSO) systems use collimated laser beams to establish point-to-point high-rate communication in space and through the atmosphere. Practical FSO applications of interest include links involving High Altitude Platforms (HAPs), satellites, deep-space probes, ground stations, Unmanned Aerial Vehicles (UAVs), aircraft, and other nomadic communication partners. HAPs are now being actively investigated in a number of programmes world-wide. This surge of recent activity reflects the fruitful demand for high-speed stratospheric FSO communication platforms [1] [2] [3]. HAPs may be unmanned aeroplanes or airships (essentially balloons, termed 'aerostats') with autonomous operation that is coupled with remote control from the ground [4]. The platforms are designed to operate in the stratosphere at typical altitudes between 18 and 27km [2] [3]. The impact of atmosphere and other significant factors reducing the performance of FSO inter-HAP communication links has been extensively studied in [5] [6] [7] [8]. An example of an inter-HAP communication network scenario is depicted in **Figure 1**.

Figure 1: Inter-HAP communication network

The performance of inter-HAP communication links is impaired by atmospheric turbulence known as scintillation: The intensity and phase of the laser light are subject to random fluctuations due to refractive index variations of atmospheric cells along the propagation path [1]. Consequently, fluctuations of received power at the receiver result in power fades and surges as shown in **Figure 4** and **Figure 5**. Often, perfect Channel State Information (CSI) is assumed to tune transmitter coding operation. However, in practical scenarios the CSI is heavily delayed due to the channel propagation time. This delay is in the order of milliseconds and therefore similar to the channel coherence time. In our work, we denote as "delayed CSI" the feedback information available at the transmitter concerning the instantaneous power value at the receiver. This information is delayed by signal propagation between receiver and transmitter. Hybrid Automatic Repeat reQuest (HARQ) is a feedback-based technique combining pure ARQ with Forward Error Correction (FEC) used with CSI to adapt the FSO transmissions to channel conditions.to increase performance [9] [10].

In this paper, we investigate and analyse the performance of adaptive code rate HARQ schemes in the presence of perfect and delayed CSI at the transmitter. The CSI is used to vary the code rate of a Reed-Solomon (RS) FEC according to the depth of channel fading. The inter-HAP system model is investigated for log normal fading channels with different fading strengths and for different coherence times induced by varying stratospheric orthogonal wind speeds. We consider direct (incoherent) detection at the receiver side with an APD receiver front end [11]. Finally, we present simulation results in terms of transmission efficiency.

The remainder of this paper is organized as follows: The system including inter-HAP scenarios, turbulence and fading channels is described in **Section 2**. In **Section 3,** the adaptive code rate HARQ mechanism using delayed CSI is described. Simulation environment and perfor-

ISBN 978-3-8007-4219-6

mance analysis are described in **Section 4**. Simulation results are presented and discussed in detail in **Section 5**. Finally, **Section 6** concludes this paper.

2 System Description

We consider the communication between two HAPs through a turbulent FSO channel. The effect of atmospheric index of refraction turbulence between HAPs is depicted in **Figure 2**. This turbulence causes fluctuations of the power at the receiver known as *Scintillations*. The combined effects of fading and temporal variations due to orthogonal stratospheric wind speeds across the FSO link are investigated.

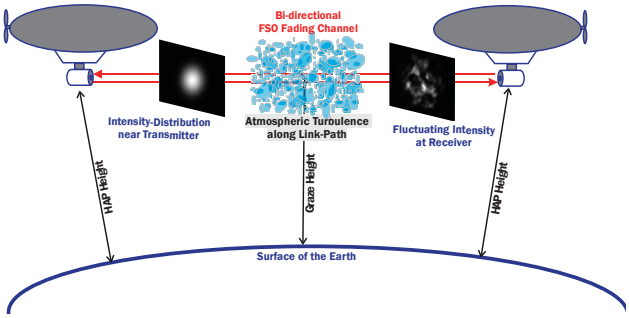

Figure 2: Inter-HAP scenario

2.1 Scenarios

The investigated scenarios for this paper are presented in Table 1. We consider basically two distances ***A*** and ***B*** of *300km* and *600km* at HAP heights (H_{hap}) of *19.76km* and *25.04km* respectively. Both scenarios have the same graze height (G_h) of *18km* which is minimum height of the optical link above the surface of the earth in the middle of the link where the turbulence strength is maximum.

Scenario	L (km)	H_{hap} (km)	G_h (km)	v (m/s)	τ_0 (ms)	PSI
A.1	300	19.76	18	10	10.95	0.42
A.2				50	2.7	0.39
B.1	600	25.04		10	13.75	0.87
B.2				50	2.75	0.97

Table 1: Bi-directional Inter-HAP scenarios.

(**Note:** The difference in PSI (Power Scintillation Index) values for the same link distances are statistical variation due to the difference in length of the vectors. However the fading strengths are similar.)

From Table 1 we see that scenarios ***A*** and ***B*** are subdivided into ***A.1***, ***A.2*** and ***B.1***, ***B.2*** based on the wind speed (v) in the stratosphere orthogonal to the optical link influencing the correlation time (τ_0) of the channel. These values are the expected minimum and maximum values for stratospheric wind speeds based on [4] [12]. The scenarios chosen for this paper will investigate joint influence of atmospheric turbulence with two different PSI (Power Scintillation Index) strengths described in *Section 2.3* around 0.4 and 0.9 with different correlation lengths of the channel due to orthogonal wind speeds.

2.2 Optical Turbulence and Path Profile

Atmospheric turbulence is often characterized by the parameter C_n^2 (in units of $m^{-2/3}$), called the refractive index structure parameter. The altitude profile for the C_n^2 parameter is calculated using the Hufnagel-Valley (H-V) model [1] given by

$$C_n^2(h) = 0.00594\left(\frac{w}{27}\right)^2 (10^{-5}h)^{10}\, exp\left(-\frac{h}{1000}\right) + 2.7\times 10^{-16}\, exp\left(-\frac{h}{1500}\right) + A exp\left(-\frac{h}{100}\right) \quad (1)$$

where, h is the altitude of the link in meters, w is the RMS wind speed (pseudo wind) in m/s and A is the value of C_n^2 at h=0 in $m^{-2/3}$. In our calculations, we use the H-V model with $w = 21\ m/s$ and A = $1.7\text{x}10^{-14}$ $m^{-2/3}$, commonly known as the *H-$V_{5/7}$ model* [1]. The RMS wind speed shall not be confused with link orthogonal wind speed. **Figure 3** depicts the optical turbulence profile along the inter-HAP link path for 300km *(Scenario A)* and 600km *(Scenario B)*.

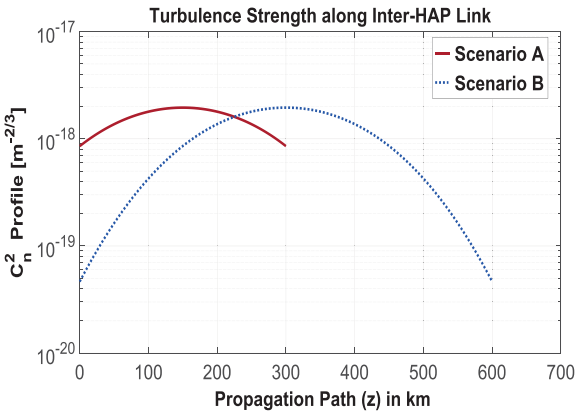

Figure 3: Turbulence strength for scenarios *A* and *B* along the propagation path.

2.3 Numerical Simulation of Fading Channel

The quantitative measure for Power Scintillation Index (PSI) σ_P^2 ,i.e., the variance of normalized received power fluctuations P_{rx} , is given by

$$\sigma_P^2 = \frac{< P_{rx}{}^2 >}{< P_{rx} >^2} - 1 \quad (2)$$

where, $< P_{rx} >$ is the temporal mean power measured at the receiver. Based on the scenarios described in **Table 1**, we generate time series of the received power vector P_{rx} also known as the fading vector.

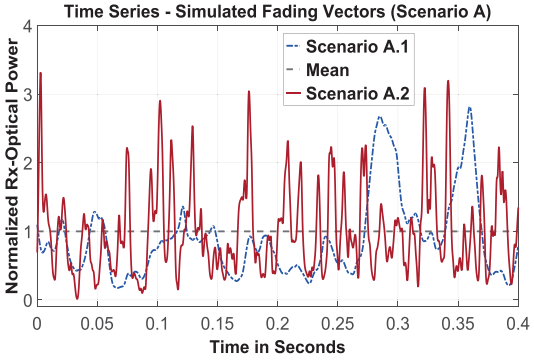

Figure 4: First 400ms of PILAB simulated vectors of *Scenario A*. Dotted line: σ_P^2 = 0.42 and $\tau_{0A.1}$ = 10.95ms. Solid line: σ_P^2 = 0.39 and $\tau_{0A.2}$= 2.7ms.

The simulation of the fading vectors was performed using PILAB (Propagation and Imaging Lab) a Matlab based programming environment developed at DLR to support simulation of FSO communication scenarios [13] [14]. PILAB uses atmospheric propagation simulations in which the dynamic of the atmospheric turbulence is modelled by phase screens that are shifted according to the transverse wind. We choose a divergence angle of 85µrad, wavelength (λ) 1550nm and a diameter (D_{rx}) of the receiver telescope of 15cm based on the link budget in Table 2 from [7].

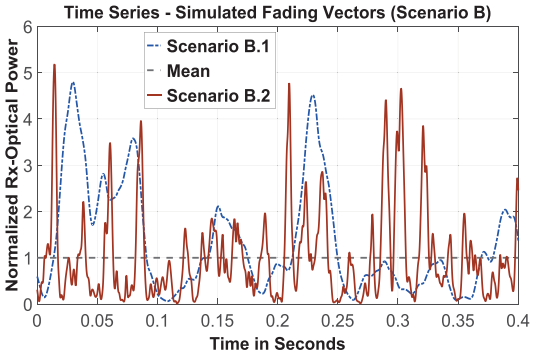

Figure 5: First 400ms of PILAB simulated vectors of *Scenario B*. Dotted line: σ_P^2 = 0.87 and $\tau_{0B.1}$ = 13.75ms. Solid line: σ_P^2 = 0.97 and $\tau_{0B.2}$= 2.75ms.

Figure 4 and **Figure 5** shows time series of simulated fading vectors using PILAB illustrating fading and timely behaviour of inter-HAP scenarios. Each of the scenarios *A* and *B* uses two different orthogonal wind speeds 10m/s and 50m/s resulting in different correlation times for the same fading channel.

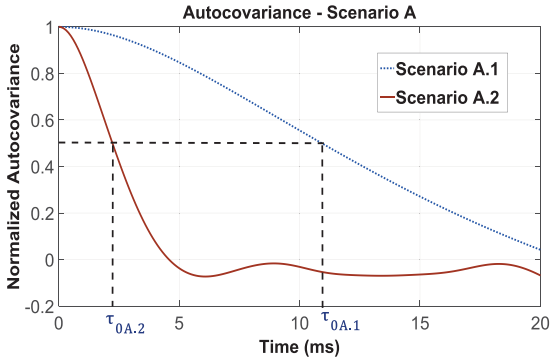

Figure 6: Autocovariance of the simulated vector for *Scenario A.1* and *Scenario A.2* with correlation time $\tau_{0A.1}$ = 10.95 ms and $\tau_{0A.2}$ = 2.7ms respectively.

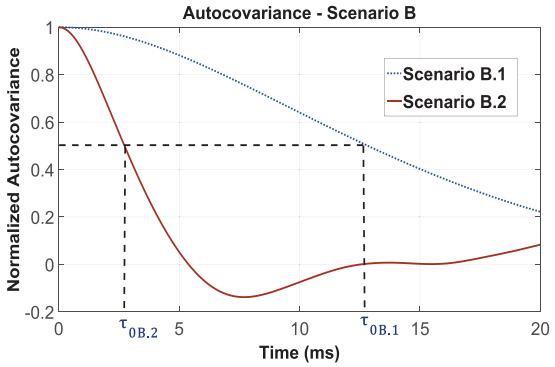

Figure 7: Autocovariance of the simulated vector for *Scenario B.1* and *Scenario B.2* with correlation time $\tau_{0B.1}$ = 13.75ms and $\tau_{0B.2}$ = 2.75ms respectively.

In this paper, the whole investigation of HARQ with CSI is performed for inter-HAP scenarios with combined effect of different PSI strengths and different temporal behaviour of the channel. **Figure 6** and **Figure 7** show the autocovariance calculated from PILAB simulated vectors. We define the correlation time for normalized autocovariance of Half-Width at Half Maximum (HWHM).

2.4 Receiver Front End (RFE)

We consider a Receiver Front End (RFE) which receives optical signal power and converts the optically On-Off Keying (OOK) modulated signal to electrical signal current by direct detection with internal gain APD (Avalanche Photo Detector). The RFE model used here is a typical APD with shot noise limited slope with Non-Return-to-Zero (NRZ) modulation, equal probability of zeros and ones, and a sensitivity $\overline{P}_{Q=2}$ based on [11]. The characteristic of binary RFEs based on the relationship between $\overline{P}_{rx}$, the BER-function, and the Q-factor can be described as

$$BER = 0.5\, erfc\left(\frac{Q(\overline{P}_{rx})}{\sqrt{2}}\right) \tag{3}$$

The Q-factor can be expressed as function of mean received power given by [11]

$$Q(\overline{P}_{rx}) = 2\left(\frac{\overline{P}_{rx}}{\overline{P}_{Q=2}}\right)^{n} \quad (4)$$

where, $\overline{P}_{Q=2} = 27.75nW$ is receiver sensitivity to achieve a $\overline{BER}$=0.023, $n = 0.5$ is the exponent determining sensitivity slope operating data rate of $R = 1.25Gbps$. For detailed overview of different RFE models the reader is referred to Table III in [11].

3 Adaptive Hybrid ARQ with Channel State Information (CSI)

In a conventional Type-I based HARQ scheme [10], the transmitter encodes the K information bytes at code rate R, and then keeps sending the same encoded packet (length N bytes) in every retransmission. The receiver only decodes the most recently received packet a gives feedback via ACK accordingly. This loop continues until successful reception of ACK at the transmitter, or the maximum retransmissions limit is reached. Whereas in a conventional Type-II based HARQ scheme [10], retransmissions generally consist only of parity bits. The receiver then combines the additional parity bits from the retransmission with the bits of the first transmission before FEC decoding is done.

The benefits of SR-ARQ scheme with a fixed rate RS-FEC for inter-HAP fading channels were studied in [6] [7]. In the present paper, we precisely vary and adapt the code rate of the RS code at the transmitter based on the available CSI. In our investigation, we consider a Type-I adaptive HARQ. We have chosen Selective Repeat (SR) ARQ scheme together with Reed-Solomon (RS) code as Forward Error Correction (FEC).

3.1 System Description

Figure 8 shows the block diagram of our proposed adaptive code rate HARQ system for inter-HAP communication link.

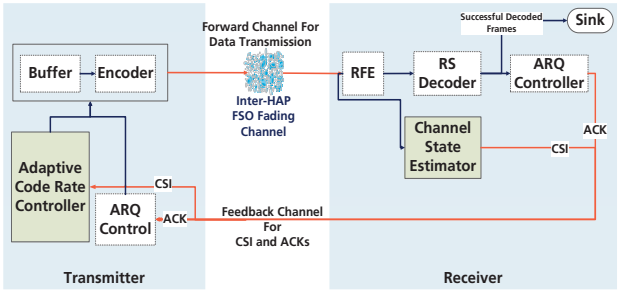

Figure 8: System model for adaptive rate HARQ + CSI

The transmitter consists of an encoder for RS-FEC, a buffer storing packets for ARQ re-transmission, ARQ control, and an adaptive code rate controller. The receiver consists of an RFE module, an RS decoder, an ARQ controller, a frame sink (destination) and a channel-state estimator. The channel used here is the inter-HAP fading channel as detailed in **Section 2**. The forward channel is only used for data transmission and the backward channel acts as the feedback channel for ACK and CSI transmission. We assume an error free backward channel for our analysis to focus on the adaptive HARQ effects in the forward channel. In a real-world system implementation, errors in the backward channel could be strongly mitigated by a strong coding and repeated transmission of the ACKs. The transmitted packets are monitored by a timer-based ARQ control module. The adaptive code rate controller tunes the RS encoding according to the CSI received. The encoded packets are transmitted via the FSO fading channel. At the receiver, the RFE detects the received signal and generates an electrical signal corresponding to the received optical irradiance. The instantaneous optical power over the receiver aperture is recorded at the channel state estimator module to provide CSI to the transmitter. The CSI is transmitted via the backward channel to the adaptive rate controller module at the transmitter that varies the code rate of RS-FEC. The successfully decoded packets are forwarded from the RS decoder block to the sink module (packet destination). For each successful decoded packet, the ARQ controller sends a corresponding ACK to the transmitter. The ARQ control at the transmitter deletes the ACKed packets from the buffer. In case of a missing ACK, the corresponding packet timer expires at the transmitter. In this case, the corresponding packet is again taken from the buffer, encoded with the current code rate, and re-transmitted. The packets are encoded with the code rate based on the CSI for each transmission and re-transmission.

3.2 Adaptive Code Rate Concept

The code rate selection plays an important role for the system to achieve a maximum throughput. We consider *eight* different code rates between no redundancy (i.e., no RS coding at all) and the maximum redundancy at which the packets can be encoded.

The operation of adaptive code rate is based on the CSI feedback from the receiver. We consider the per packet instantaneous received optical power $P_{rx}(t)$ at the RFE as the CSI. This CSI at the receiver is sent back to the transmitter via the backward channel (assumed to be error free) and the RS code rate adaption is executed accordingly for the next transmission or re-transmission at the transmitter. The code rate R is adapted according to a Look-Up Table (LUT) as shown in **Table 2** that translates the CSI information ($P_{rx}(t)$) to the code rate R. This table was generated from simulations of a non-fading channel to obtain the maximum possible Transmission Efficiency (TE) based on the code rate R for each instantaneous power value $P_{rx}(t)$. For all transmissions we assume a constant length of the code word N of 255bytes; the rate change is obtained by changing the length of redundancy (N-K) bytes.

t	R	$\overline{P}_{rx}$ (nW)	BEP	SEP	SEP after FEC	PEP after FEC
0	**1**	∞	0	0	0	0
		117	2.0 E-05	1.6 E-04	7.4 E-13	5.9 E-12
4	**0.96**	65.5	1.1 E-03	8.7 E-03	2.0 E-04	1.6 E-03
8	**0.94**	56.5	2.2 E-03	1.7 E-02	3.3 E-07	2.6 E-06
16	**0.87**	43	6.4 E-03	5.0 E-02	2.4 E-07	1.9 E-06
32	**0.75**	33.6	1.3 E-02	1.0 E-01	3.6 E-06	2.9 E-05
48	**0.62**	27.6	2.3 E-02	1.7 E-01	8.6 E-05	6.9 E-04
64	**0.5**	23.65	3.2 E-02	2.3 E-01	2.0 E-04	1.7 E-03
80	**0.375**	0	0.5	9.9 E-01	1	1

Table 2: LUT for optimum code rate selection, 1 symbol is 8 bits. *t* is maximum number of correctable symbol errors by RS-FEC in bytes.

(**Note:** The P_{rx} column represents a range of mean received power for its corresponding code rate R. The SEP and PEP after RS-FEC are chosen for the lower rate.)

4 Performance Analysis

4.1 Transmission Efficiency (TE)

We quantitatively evaluate the performance of HARQ with adaptive RS FEC in terms of the *Transmission Efficiency (TE)* defined as the fraction of the channel bit rate usable for payload transport [10]. The TE is evaluated under the following assumptions:

(1) The feedback/ backward channel are considered as error free. This channel is used for ACK and CSI transmissions.
(2) All channel errors are detected.
(3) The maximum number of re-transmissions for a packet is unlimited, i.e., the transmitter retransmits a packet until successful decoding at the receiver.
(4) The performance comparison is performed for adaptive rate HARQ and cases with perfect and delayed CSI. Also, we show comparison plots for fixed rate HARQ schemes.
(5) Perfect CSI (P-CSI) means that the current CSI at the receiver is immediately available at the transmitter. Delayed CSI (D-CSI) refers to the fact that the CSI is delayed by the Round Trip Time (RTT) of that scenario (e.g., a link distance of 300km would delay the CSI by 2ms).
(6) The TE is shown for different mean received power of the fading channels based on the scenarios in Table 1.

4.2 Coding Gain

We quantify the results also in terms of *coding gain* in *dB*. We define it as the amount of additional mean received power $\overline{P}_{rx}$ in nW that would be required to provide the same TE for an uncoded ARQ system.

4.3 Simulation Environment

All simulation runs were performed using the OMNeT++ Discrete Event Simulator [15]. The normalized power vectors for different scenarios are imported to the RFE model within OMNeT++ to obtain the raw channel BEP. Based on this BEP the PEP is calculated and the packets are randomly destroyed accordingly. The SR-ARQ protocol with adaptive rate control is implemented in the OMNeT++ environment. The parameters used for simulation are shown in **Table 3**.

Parameter	Value	Symbol	Unit
Total Frame Length	2040	n_f	bits
Overhead	variable	n_o	bits
Window Size	2048	W_s	frames
Net Data Rate	1	R_n	Gbps
Link Distance	300/ 600	L	km
Round Trip Time	2/ 4	t_{rtt}	ms
Transmission Time for one frame	2.04	t_s	µs

Table 3: Adaptive HARQ simulation parameters

5 Results and Discussion

The results are presented in terms of TE for adaptive rate HARQ (RS+SR) with perfect and delayed CSI at the transmitter. The simulations were investigated for different mean power $\overline{P}_{rx}$ at the receiver for the fading channel. The simulations show the scenarios detailed in **Table 1**.

Figure 9 represents the simulative TE performance of fixed and adaptive code rate HARQ for a non-fading channel condition (delay of CSI is not relevant then): Here, the performance of adaptive rate HARQ is the combination of the maximum of the TE values that are achieved at the different fixed-rate FEC configurations.

ISBN 978-3-8007-4219-6

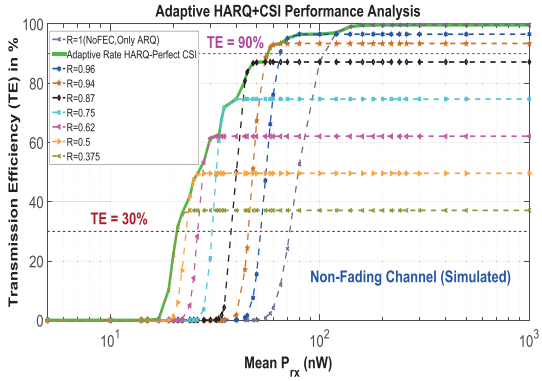

Figure 9: Performance analysis – *Non-fading channel*

Figure 10 and **Figure 11** show the performance analysis of *Scenario A.1* and *Scenario A.2* respectively. In both figures, the 'solid green line' represents adaptive rate TE for perfect CSI at the receiver and the 'solid red line' shows the adaptive rate TE for delayed CSI (2ms). Both these scenarios have the similar fading strengths but different timely behaviour as depicted in **Figure 4**. The CSI is delayed at the transmitter by 2ms (RTT) for both cases but the correlation time of *A.1* is almost 5 times shorter than *A.2*. This means that the relative CSI error increases as the channel correlation time gets closer to the CSI delay.

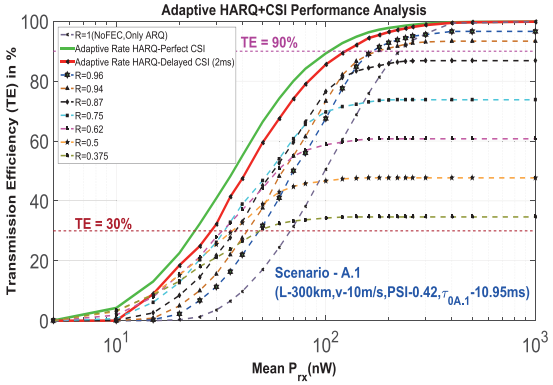

Figure 10: Performance analysis – *Scenario A.1*

In **Figure 10**, we observe that the adaptive rate TE outperforms all the fixed code rate cases except for very low powers less than 10nW for delayed CSI. Also, the coding gain slowly decreases for lower power values and we observe considerable coding gain for TE ~ above 40%. In **Figure 11**, we observe that the adaptive rate TE outperforms all the fixed code rate cases in case of perfect CSI at the transmitter. However, in the case of delayed CSI of 2ms we observe that the TE drops when $\overline{P}_{rx}$ gets below ~200nW, thus providing lower performance than the fixed rate HARQ. This effect is due to the relatively outdated CSI at the transmitter with the correlation time of the fading channel of τ_0 = 2.7ms.

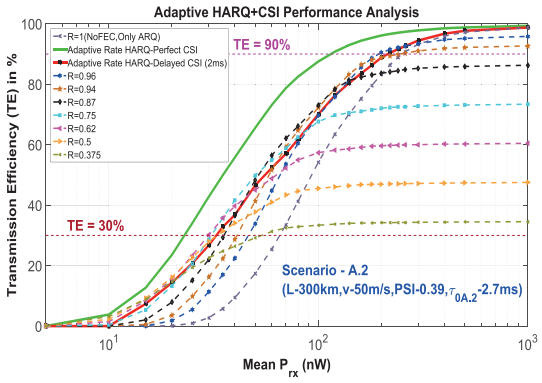

Figure 11: Performance analysis – *Scenario A.2*

Figure 12 and **Figure 13** show the performance analysis of *Scenario B.1* and *Scenario B.2* respectively. In both figures, the 'solid green line' represents adaptive rate TE for perfect CSI at the receiver and the 'solid red line' shows the adaptive rate TE for delayed CSI (4ms).

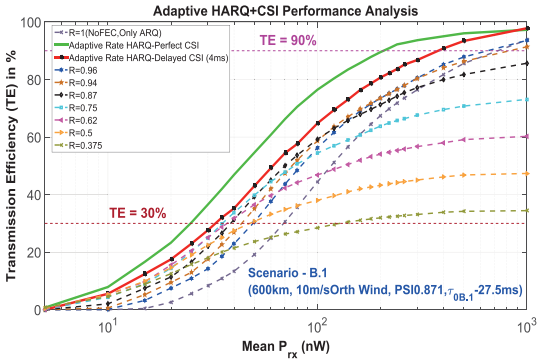

Figure 12: Performance analysis – *Scenario B.1*

Figure 12 shows the adaptive rate TE outperforming all the fixed rate scenarios at lower and higher powers. Also, we see considerable coding gain overall.

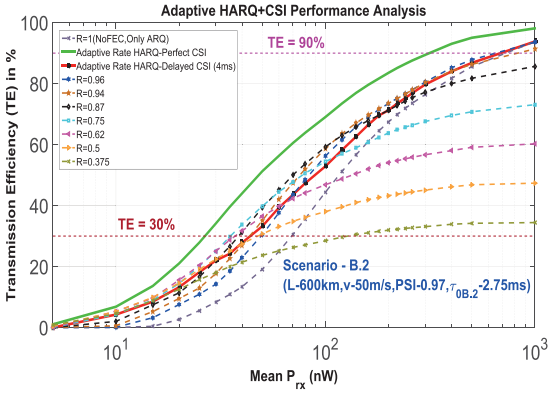

Figure 13: Performance analysis – *Scenario B.2*

In **Figure 13** we see that the TE of adaptive rate HARQ is considerably reducing compared to **Figure 12.** We also observe that adaptive rate HARQ is only as good as the fixed rate (R=0.96) HARQ for TE of 60-90%. Also, the TE of fixed code rate HARQ is better than for the adaptive at lower TE ~30%. This effect is due to increased fading strength (PSI =0.97) and reduced correlation time

(τ_0 = 2.75ms) for a CSI delay of 4ms. **Table 4** shows an overview of coding gain achieved by our adaptive rate approach in comparison with ARQ (no RS-FEC).

L (km)	v (m/s)	τ_0 (ms)	PSI	Gain (dB) for TE = 30%		Gain (dB) for TE = 90%	
				D-CSI	P-CSI	D-CSI	P-CSI
300	10	10.95	0.42	**3.6**	**4.8**	**2.6**	**3.4**
	50	2.7	0.39	**2.9**	**4.5**	**0.7**	**3.3**
600	10	13.75	0.87	**3.2**	**4.4**	**2.4**	**5.4**
	50	2.75	0.97	**1.9**	**4.1**	**0.3**	**3.6**

Table 4: Coding gain for adaptive code rate HARQ with CSI compared with ARQ (no RS-FEC) for Transmission Efficiency (TE) of 30% and 90%. Delayed CSI (D-CSI), Perfect CSI (P-CSI).

6 Conclusion and Outlook

In this paper, we investigated the effects of delayed CSI on the achievable Transmission Efficiency (TE) of adaptive rate HARQ (SR+RS-FEC) scheme for FSO inter-HAP fading channels. The considered channel had the impact of different fading strengths and correlation time. The coding gain from the adaptive rate HARQ were shown in comparison with uncoded ARQ. All the numerical simulations of HARQ were performed in OMNeT++ and the results are evaluated in terms of transmission efficiency. We identified the impact of the outdated/ delayed CSI on the overall system performance. The results showed the CSI at the transmitter plays an important role for adapting the code rate of the transmission thereby achieving maximum throughput and reducing delays due to re-transmission. We expect that CSI prediction at the transmitter will improve the overall efficiency of the system in the cases with larger CSI delay. Also, applying more efficient decoding methodology like Soft Combining (SC) at the receiver can be expected to yield an improved performance.

7 References

[1] Andrews, L.C and Phillips, R.C., "Laser Beam Propagation through Random Media - Second Edition," SPIE-Press, Bellingham, 2005.

[2] https://www.google.com/loon/

[3] https://info.internet.org/en/

[4] Tozer, T. C., Grace, D., "High-altitude platforms for wireless communications," Electron. Commun. Eng. J., 13, 127–137.2001.

[5] Giggenbach, D., Purvinskis, R., Werner, M., Holzbock, M., "Stratospheric Optical Inter-Platform Links for High Altitude Platforms," Online Proceed-ings. 20th AIAA International Communications Sa-tellite Systems Conference,2002.

[6] Parthasarathy, S., Giggenbach, D., Kirstädter, A., "Channel Modelling for Free-Space Optical Inter-HAP Links Using Adaptive ARQ Transmission". SPIE Proceedings. SPIE Security and Defence 2014, 22-25 Sep 2014, Amsterdam, Netherlands. ISBN 9781628413113

[7] Parthasarathy, S., Kirstädter, A., Giggenbach, D., "Simulative Performance Analysis of ARQ Schemes for Free-Space Optical Inter-HAP Channel Model," in Photonic Networks; 16. ITG Symposium; Proceedings of , vol., no., pp.1-5, 7-8 May 2015

[8] David, F., Giggenbach, D., Henniger, H., Horwath, J., Landrock, R. Perlot, N., "Design Considerations for Optical Inter-HAP Links," Proceedings ICSSC, 22nd AIAA International Communications Satellite Systems Conference & Exhibit, Monterey, CA, May 9-12, 2004.

[9] Li, Y., Gursoy M. C., and Velipasalar, S., "On the Throughput of Hybrid-ARQ Under Statistical Queuing Constraints," in IEEE Transactions on Vehicular Technology, vol. 64, no. 6, pp. 2725-2732, June 2015.

[10] Lin, S., Costello, D. J., "Error Control Coding: Fundamentals and Applications, " 2nd ed., Prentice Hall, 2004.

[11] Giggenbach, D., Mata-Calvo, R., "Sensitivity modeling of binary optical receivers," Appl. Opt. 54, 8254-8259 (2015).

[12] Colozza, A., "Initial Feasibility Assessment of a High Altitude Long Endurance Airship, " NASA CR-2003-212724, Dec. 2003.

[13] Horwath, J., Perlot, N., Giggenbach, D., Jüngling, R., "Numerical simulations of beam propagation through optical turbulence for high-altitude platform crosslinks". In: LASE 2004, San Jose, Vol. 5, pp. 243-248. SPIE Optical Press. Free-Space Laser Communication Technologies XVI, 2004-01-27 - 2004-01-29, San Jose, California, USA. ISBN 0-8194-5246-7. ISSN 0277-786X.

[14] Perlot, N., Horwath, J., Jüngling, R., "Modeling wind in simulations of atmospheric optical propagation". Proc. SPIE 5712, Free-Space Laser Communication Technologies XVII, 140 (May 02, 2005)

[15] https://omnetpp.org/